

# Deficient neuron-microglia signaling results in impaired functional brain connectivity and social behavior

Yang Zhan<sup>1,8</sup>, Rosa C Paolicelli<sup>1,8</sup>, Francesco Sforzini<sup>2,3</sup>, Laetitia Weinhard<sup>1</sup>, Giulia Bolasco<sup>1</sup>, Francesca Pagani<sup>4</sup>, Alexei L Vyssotski<sup>5</sup>, Angelo Bifone<sup>2</sup>, Alessandro Gozzi<sup>2</sup>, Davide Ragozzino<sup>6,7</sup> & Cornelius T Gross<sup>1</sup>

Microglia are phagocytic cells that infiltrate the brain during development and have a role in the elimination of synapses during brain maturation. Changes in microglial morphology and gene expression have been associated with neurodevelopmental disorders. However, it remains unknown whether these changes are a primary cause or a secondary consequence of neuronal deficits. Here we tested whether a primary deficit in microglia was sufficient to induce some autism-related behavioral and functional connectivity deficits. Mice lacking the chemokine receptor *Cx3cr1* exhibit a transient reduction of microglia during the early postnatal period and a consequent deficit in synaptic pruning. We show that deficient synaptic pruning is associated with weak synaptic transmission, decreased functional brain connectivity, deficits in social interaction and increased repetitive-behavior phenotypes that have been previously associated with autism and other neurodevelopmental and neuropsychiatric disorders. These findings open the possibility that disruptions in microglia-mediated synaptic pruning could contribute to neurodevelopmental and neuropsychiatric disorders.

Neurodevelopmental disorders arise early in life and are often characterized by social deficits, impaired language development, intellectual disability, increased repetitive or restricted behaviors and motor abnormalities. Cognitive impairment has an important role in these disorders, but their underlying pathophysiology remains obscure. Genetic studies have linked variation in synaptic scaffolding proteins to schizophrenia and autism<sup>1</sup>, and postmortem studies have identified decreased expression of genes associated with synaptic transmission across cortical regions in these and other disorders<sup>2,3</sup>. Furthermore, functional magnetic resonance imaging (fMRI) and electroencephalography have both pointed to decreased functional connectivity between cortical regions across a variety of diseases with cognitive deficits, including autism<sup>4–6</sup>, schizophrenia<sup>7,8</sup>, major depression<sup>9,10</sup>, epilepsy<sup>11</sup> and obsessive compulsive disorder<sup>12</sup>. Together these data suggest that deficits in synaptic maturation that are characterized by weak functional connectivity across brain regions may have a role in the pathophysiology of multiple mental illnesses<sup>13</sup>.

In the case of autism, several theories have been put forward that describe circuit-level deficits in the disorder, including the weak central coherence model<sup>14</sup>, the underconnectivity model<sup>15</sup> and the enhanced excitatory-inhibitory balance model<sup>16</sup>. So far, however, the developmental mechanisms that might give rise to such connectivity deficits have not been described. Here we investigated the possibility that deficits in the elimination of synapses during synaptic maturation, so-called ‘pruning’, might explain some of the behavioral

and circuit-level deficits found in autism. Microglia have a critical role in pruning synapses during development<sup>17</sup>. Microglia are non-neuronal cells that derive from embryonic myeloid precursors, take up residence in the brain during development and actively phagocytose synapses during the period of rapid synapse formation and elimination<sup>18–20</sup>. Mice that have a transient reduction of microglia in the brain due to a failure to respond to the neuronally expressed chemokine fractalkine (fractalkine receptor knockout mice, *Cx3cr1*<sup>KO</sup>) show an excess of weak excitatory synapses as a consequence of their failure to eliminate immature synaptic connections during the second and third postnatal weeks<sup>19</sup>. In wild-type mice, this period of synaptogenesis is associated with a rapid increase in the amplitude of spontaneous excitatory postsynaptic currents (sEPSCs), a feature that likely reflects an increase in synaptic multiplicity (number of synapses per axonal input) resulting from the local sprouting of synaptic connections<sup>21,22</sup>. The amplitude of miniature excitatory postsynaptic currents (mEPSCs), conversely, reflects non-action potential-dependent release of synaptic vesicles at individual synapses and remains constant over this developmental period<sup>21,22</sup>. In *Cx3cr1*<sup>KO</sup> mice, excitatory inputs fail to show increased sEPSC amplitudes at postnatal day (P) 15 (ref. 19), suggesting immature synaptic multiplicity. However, it is not known whether synaptic multiplicity remains abnormal in adult *Cx3cr1*<sup>KO</sup> mice, although it has been shown that these mice have hippocampus-dependent behavioral deficits<sup>23</sup>. Here we show that reduced synaptic pruning during development is associated with persistent deficits in synaptic multiplicity, reduced functional connectivity between brain

<sup>1</sup>Mouse Biology Unit, European Molecular Biology Laboratory (EMBL), Monterotondo, Italy. <sup>2</sup>Center for Neuroscience and Cognitive Systems @UniTn, Istituto Italiano di Tecnologia (IIT), Rovereto, Italy. <sup>3</sup>Institutions Markets Technology (IMT) Institute for Advanced Studies, Lucca, Italy. <sup>4</sup>Center for Life Nano Science, IIT, La Sapienza University, Rome, Italy. <sup>5</sup>Institute of Neuroinformatics, University of Zürich and Swiss Federal Institute of Technology (ETH), Zurich, Switzerland. <sup>6</sup>Department of Physiology and Pharmacology, La Sapienza University, Rome, Italy. <sup>7</sup>Istituto di Ricovero e Cura a Carattere Scientifico (IRCCS) Neuromed, Pozzilli, Italy. <sup>8</sup>These authors contributed equally to this work. Correspondence should be addressed to C.T.G. ([gross@embl.it](mailto:gross@embl.it)).

Received 23 July 2013; accepted 2 January 2014; published online 2 February 2014; doi:10.1038/nn.3641

regions, impaired social interaction and increased grooming behavior. These findings demonstrate a causal role for microglia in the maturation of functional brain connectivity and open the possibility that a primary deficit in microglia may contribute to circuit-level deficits across neurodevelopmental disorders, including autism.

## RESULTS

### Persistent deficit in excitatory synapse maturation

To determine whether immature synaptic multiplicity persisted in *Cx3cr1*<sup>KO</sup> animals in adulthood, we measured sEPSCs and mEPSCs in CA1 pyramidal neurons in hippocampal slices at P40 (Supplementary Fig. 1a–g), when microglia and dendritic spine density in knockout mice had reached wild-type levels<sup>19</sup>. Wild-type mice at P40 showed significantly larger sEPSC than mEPSC amplitudes (Fig. 1a,b), whereas sEPSC and mEPSC amplitudes were similar in *Cx3cr1*<sup>KO</sup> littermates (Fig. 1c,d). These results demonstrate that synaptic multiplicity in *Cx3cr1*<sup>KO</sup> mice remains significantly decreased in adulthood despite normal spine density. Consistent with our observation of a transient increase in spine density in knockout mice<sup>14</sup>, mEPSC frequency increased to a greater extent from P15 to P40 in wild-type mice than in knockout mice (Fig. 1e,f), and the mEPSC frequency at P40 was similar between genotypes (*t* test; wild type:  $2.5 \pm 0.2$  Hz (mean  $\pm$  s.e.m.),  $n = 16$ ; KO:  $2.3 \pm 0.4$  Hz,  $n = 12$ ;  $t_{26} = 0.32$ ,  $P = 0.75$ ). These findings show that a transient reduction in microglia results in a long-term deficit in synaptic multiplicity despite normal excitatory synapse number and suggest that there is a critical window during which microglia-mediated synaptic pruning is essential for proper circuit maturation.

To understand whether microglia-mediated pruning selectively affected excitatory inputs, we measured miniature inhibitory postsynaptic currents (mIPSCs) in CA1 hippocampal pyramidal neurons at P15, an age at which mEPSC frequency was significantly increased in knockout mice<sup>19</sup>. The frequency of mIPSCs was moderately higher in wild-type mice when compared to *Cx3cr1*<sup>KO</sup> littermates (Supplementary Fig. 1h), demonstrating that inhibitory and excitatory synapses are differentially affected in *Cx3cr1*<sup>KO</sup> mice and suggesting that inhibitory synapses may not be substrates for microglia-mediated synaptic pruning.

### Morphological substrates of synaptic multiplicity

The increase in synaptic multiplicity observed at Schaffer collateral synapses during postnatal development has been proposed to depend on an increase in release sites connecting individual CA3 and CA1 neurons<sup>21</sup>. However, no morphological evidence for such changes has been reported, and it remains unclear whether they reflect an increase in the size of the readily releasable pool of synaptic vesicles within single synapses or an increase in the number of synaptic contacts between pairs of CA3-CA1 neurons. To identify morphological substrates of differential Schaffer collateral synaptic multiplicity, we quantified the synaptic ultrastructure in electron micrographs of CA1 stratum radiatum from *Cx3cr1*<sup>KO</sup> and wild-type littermates at P40. The number of total, reserve and docked synaptic vesicles in the excitatory synapses was unaltered in the knockout mice (Fig. 1g), arguing against a difference in the size of the readily releasable pool in individual excitatory synapses. We observed that the majority of boutons made excitatory synapses onto a single postsynaptic spine.

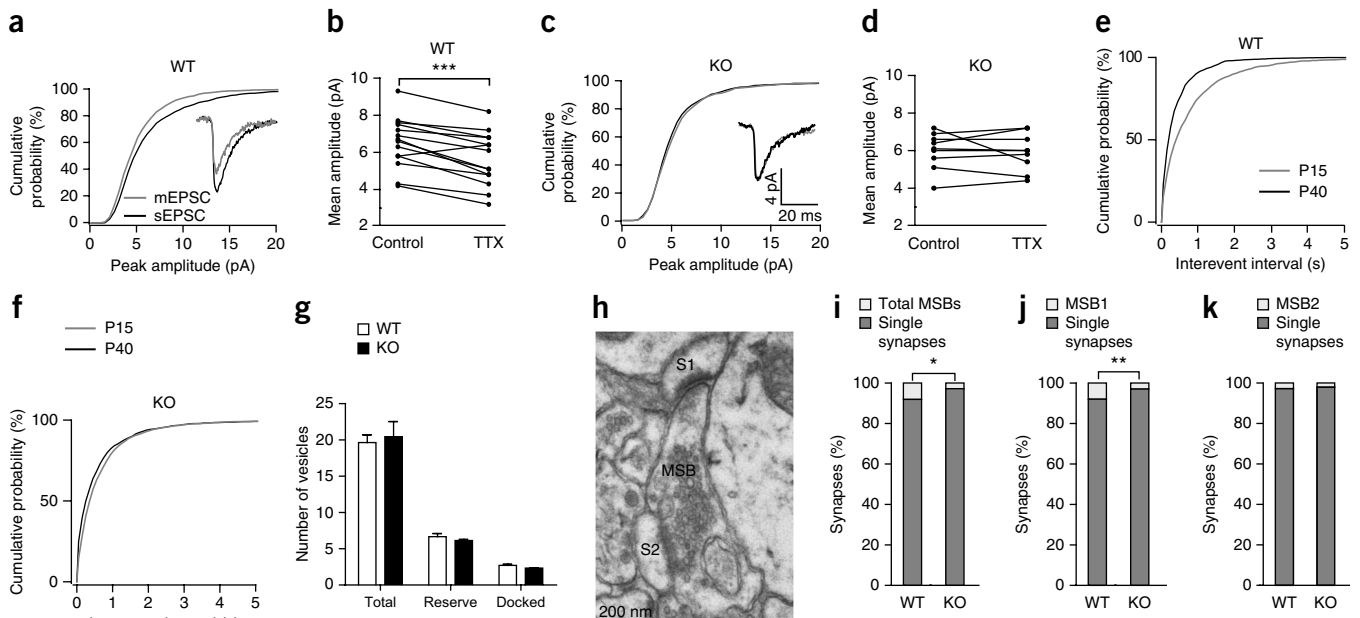


**Figure 1** Deficient synaptic multiplicity in *Cx3cr1*<sup>KO</sup> mice. (a–h) Whole-cell recordings of CA1 pyramidal cells in brain slices from wild-type (WT) and *Cx3cr1*<sup>KO</sup> (KO) littermates. (a,c) Cumulative distributions of sEPSC (no tetrodotoxin (TTX), black line) and mEPSC (0.5–1  $\mu$ M TTX, gray line) amplitudes at P40 in neurons from wild-type and knockout mice (WT:  $n = 14$ ,  $D = 0.1$ ,  $P < 0.0001$ ; KO:  $n = 9$ ,  $D = 0.05$ ,  $P = 0.18$ ). (b,d) sEPSC and mEPSC mean amplitudes in neurons from wild-type (paired *t* test; control:  $6.5 \pm 0.4$  pA (mean  $\pm$  s.e.m.); TTX:  $5.6 \pm 0.4$  pA;  $n = 14$ ;  $t_{13} = 5.4$ ,  $P < 0.001$ ) and knockout (control:  $5.9 \pm 0.3$  pA; TTX:  $5.7 \pm 0.3$  pA;  $n = 9$ ;  $t_8 = 0.75$ ,  $P = 0.47$ ) littermates at P40. (e,f) Cumulative distributions of the mEPSC interevent intervals at P15 (gray line) and P40 (black line) in wild-type compared to *Cx3cr1*<sup>KO</sup> littermates (WT, P15:  $n = 20$ , P40:  $n = 16$ ,  $D = 0.21$ ,  $P < 0.0001$ ; KO, P15:  $n = 26$ , P40:  $n = 12$ ,  $D = 0.12$ ,  $P < 0.0001$ ). (g) Electron microscopy quantification of vesicles (total, reserve (<50 nm from the synaptic cleft) and docked) per synapse in wild-type and knockout littermates at P40. Error bars, s.e.m. (h) Representative electron micrograph of an MSB contacting two dendritic spines (S1 and S2). (i) The fraction of single-synapse boutons as compared to MSBs in knockout mice compared to wild-type littermates ( $\chi^2$  test; WT:  $n = 199$  boutons; KO:  $n = 182$  boutons). (j,k) Serial-section electron microscopy quantification of MSBs contacting spines emanating from the same (MSB1) dendritic target ( $\chi^2$  test; WT:  $n = 346$  boutons; KO:  $n = 282$ ; j) and MSBs contacting spines from different (MSB2) dendritic targets (WT:  $n = 327$ ; KO:  $n = 280$ ,  $P = 0.63$ ; k) in wild-type compared to *Cx3cr1*<sup>KO</sup> mice. \* $P < 0.05$ , \*\* $P < 0.01$ , \*\*\* $P < 0.001$ .

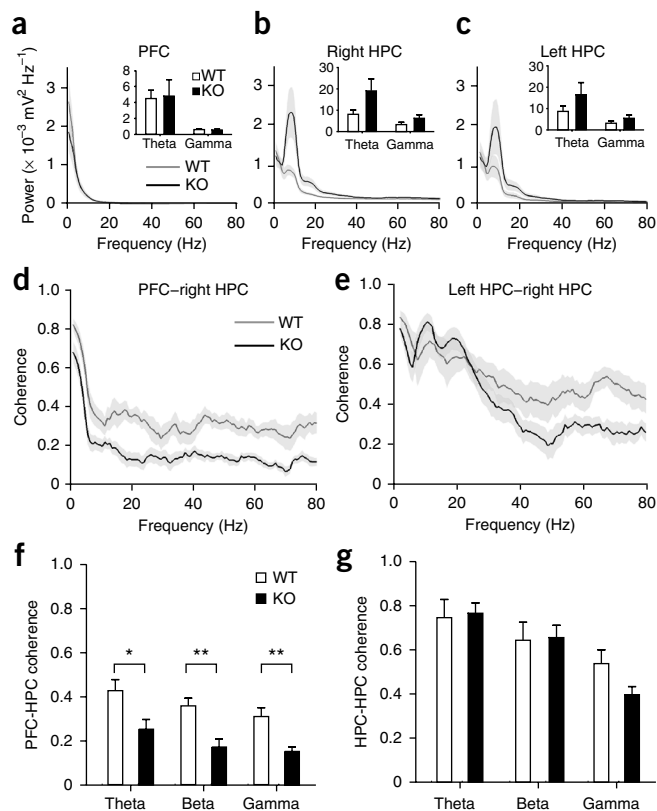
**Figure 2** Reduced LFP functional connectivity in *Cx3cr1*<sup>KO</sup> mice. (a–c) Average power spectra obtained for LFP recordings in the medial PFC (WT: *n* = 7, KO: *n* = 10; a), the right dorsal HPC (WT: *n* = 7, KO: *n* = 10; b) and the left dorsal HPC (WT: *n* = 7, KO: *n* = 9; c) in alert wild-type and *Cx3cr1*<sup>KO</sup> mice during exploration of a novel environment. The insets show the mean power in the theta (4–12 Hz) and gamma (26–70 Hz) bands, which did not differ significantly between genotypes, although a trend for an increase was seen in knockout mice for theta power in the right (*t* test;  $t_{15} = 1.6$ ,  $P = 0.13$ ) and left (*t* test;  $t_{14} = 1.1$ ,  $P = 0.28$ ) HPC. (d–g) Coherence between LFP signals recorded from PFC and the right HPC (WT: *n* = 7, KO: *n* = 10; d) and the left and right HPC (WT: *n* = 7, KO: *n* = 9; e) in *Cx3cr1*<sup>KO</sup> mice compared to wild-type littermates, as well as coherence in the theta (4–12 Hz), beta (15–25 Hz) and gamma (26–70 Hz) bands in PFC-HPC (WT: *n* = 7, KO: *n* = 10; f) and in the gamma band (*t* test;  $t_{14} = 2.05$ ,  $P = 0.06$ ) in HPC-HPC (WT: *n* = 7, KO: *n* = 9; g). \* $P < 0.05$ , \*\* $P < 0.01$ . Error bars (a–c, f, g), s.e.m. In a–e, the curves and shaded areas indicate the mean  $\pm$  s.e.m.

In wild-type animals, about 10% of boutons made excitatory synapses onto two postsynaptic spines (Fig. 1h), so-called multisynapse boutons (MSBs)<sup>24</sup>. Strikingly, in knockout mice, MSBs made up less than 5% of boutons, which was significantly less than in wild-type littermates (Fig. 1i).

To identify the subset of MSBs that made contacts onto spines emanating from the same dendrite and were therefore capable of contributing to synaptic multiplicity, we quantified synaptic boutons in serial-section electron micrographs in which spine architecture could be fully reconstructed (Supplementary Fig. 2c–h). Whereas the majority of MSBs in wild-type mice made contact with spines from the same dendrite (so-called MSB1s), a significantly smaller fraction of MSBs in knockout mice made such contacts (Fig. 1j). Notably, the fraction of MSBs that made contact with two dendrites (so-called MSB2s) did not differ between the genotypes (Fig. 1k). These data demonstrate that MSBs are an important source of synaptic multiplicity in the Schaffer collateral pathway and suggest that deficient synaptic multiplicity in *Cx3cr1*<sup>KO</sup> mice may be driven, at least in part, by a failure of CA3 axons to form MSBs onto CA1 target neurons. To test the possibility that there might be an increase of Schaffer collateral afferents as a result of deficient pruning, we quantified the density of axonal segments in CA1 stratum radiatum. These data revealed that axonal segment density is unaltered in knockout mice (Supplementary Fig. 2a, b) and suggest that synaptic pruning in the Schaffer collateral pathway involves the removal of synaptic boutons without the elimination of axons.

### Reduced functional brain connectivity

The reduced synaptic multiplicity seen in *Cx3cr1*<sup>KO</sup> mice suggested that gross connectivity between brain regions might be weakened. To quantify long-range functional connectivity, we measured the coherence of local field potentials (LFPs; Supplementary Fig. 3a) between the right and left dorsal hippocampus (HPC; Supplementary Fig. 4a, c) and the medial prefrontal cortex (PFC; Supplementary Fig. 4b, d) in awake behaving *Cx3cr1*<sup>KO</sup> and wild-type littermates<sup>25</sup>. Although power spectra for the LFP signals in all three structures did not differ significantly (right HPC: *t* test, theta power,  $t_{15} = 1.6$ ,  $P = 0.13$ ; gamma power,  $t_{15} = 1.4$ ,  $P = 0.19$ . PFC: *t* test, theta power,  $t_{15} = 0.1$ ,  $P = 0.91$ ; gamma power,  $t_{15} = 0.93$ ,  $P = 0.36$ . Left HPC: *t* test, theta power,  $t_{14} = 1.1$ ,  $P = 0.28$ ; gamma power,  $t_{15} = 1.3$ ,  $P = 0.2$ ) between genotypes (Fig. 2a–c), coherence spectra indicated a significant decrease in functional connectivity between PFC and HPC across a wide frequency range (Fig. 2d, f) and a trend for a decrease in functional connectivity between the left and right HPC in the gamma band (Fig. 2e, g). Notably, PFC-HPC coherence and



power were not modulated appreciably by the speed of the animal (Supplementary Fig. 3b–d).

Next we assessed global functional connectivity by quantifying the synchronization of blood oxygen level-dependent (BOLD) fMRI signals across brain regions in anesthetized wild-type and *Cx3cr1*<sup>KO</sup> mice<sup>26–28</sup>. The synchronization of BOLD signals in PFC and HPC was significantly decreased in knockout mice when compared to wild-type littermates (Fig. 3a, b), whereas the synchronization between the left and right HPC was not significantly ( $P = 0.6$ ) altered (Fig. 3c), which matches the pattern of functional connectivity deficits seen using LFP coherence (Fig. 2f, g). We detected no significant confounding effect of genotype on depth of anesthesia during fMRI as assessed by the magnitude of BOLD signal fluctuation<sup>29</sup> ( $P = 0.47$ ; Supplementary Fig. 5a) or mean arterial blood pressure ( $P = 0.41$ ; Supplementary Fig. 5b)<sup>30</sup>. A broader analysis of fMRI data indicated that the genotype difference in PFC-HPC synchronization exhibited a gradient across the dorsal-ventral hippocampal axis (Supplementary Fig. 6a), with greater differences being seen in the ventral hippocampus, a region that makes direct connections with PFC<sup>31</sup>. To validate the gradient of functional connectivity deficits across the hippocampus, we repeated our LFP coherence study with electrodes placed simultaneously in the dorsal and ventral hippocampus. Consistent with the fMRI synchronization data, LFP coherence deficits in knockout mice were greater in the ventral than in the dorsal hippocampus (Supplementary Fig. 6b–e), corroborating the hypothesis that the two methodologies reflect a common underlying functional connectivity deficit in knockout mice. Moreover, analysis of global BOLD signal synchronization revealed widespread deficits in functional connectivity in knockout mice. In particular, functional connectivity between PFC and several brain structures, including the hippocampus, nucleus accumbens and temporal association cortex, was reduced in knockout mice when compared to wild-type littermates (Fig. 3d–g

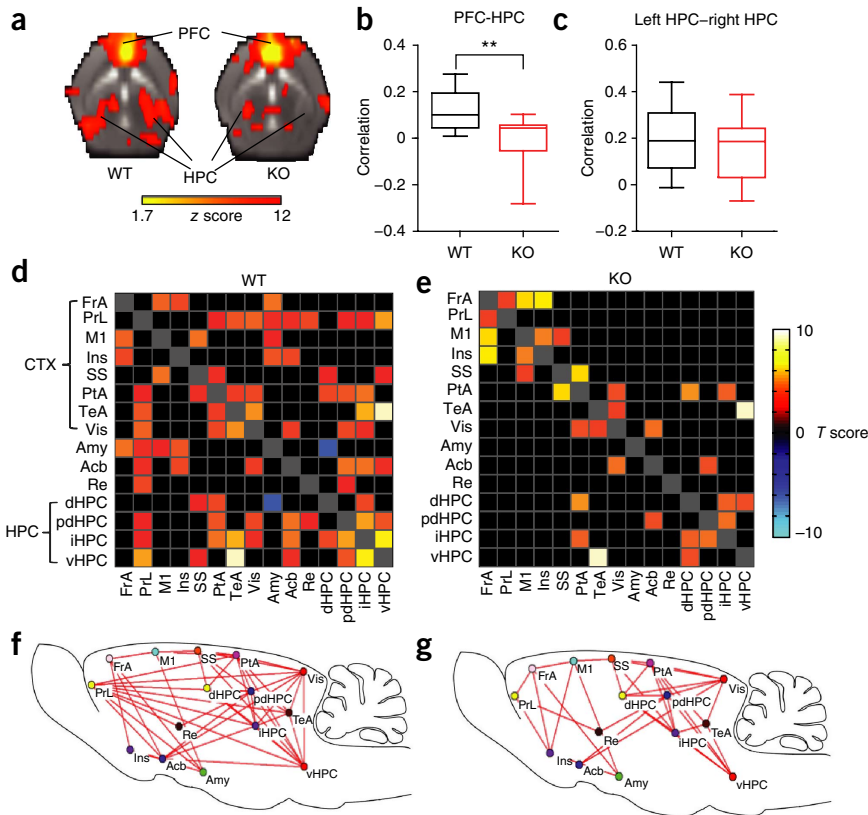


**Figure 3** Decreased fMRI functional connectivity in *Cx3cr1*<sup>KO</sup> mice. **(a)** Transverse brain section heat maps showing mean voxels for which the fMRI BOLD signal was significantly correlated with PFC (the z score indicates the strength of the correlation). **(b,c)** PFC correlations (measured by BOLD synchronization) in PFC-HPC (*t* test;  $t_{14} = 2.3$ ,  $P = 0.005$ ; **b**) and left HPC-right HPC (*t* test;  $t_{14} = 0.55$ ,  $P = 0.6$ ; **c**) in *Cx3cr1*<sup>KO</sup> mice and wild-type littermates. **(d,e)** Correlation matrices derived from global fMRI BOLD signal analysis (pseudocolor map of *t* statistics after thresholding at a false discovery rate *q* of 0.05) revealing widespread reductions in functional connectivity across brain regions in knockout compared to wild-type mice (the brain region abbreviations are defined in **Supplementary Fig. 6b**). **(f,g)** Superposition of the most prominent fMRI BOLD correlations between brain regions on the mouse brain highlighting the preferential reduction in connectivity between distant brain regions and PFC. PrL, prelimbic cortex. For all panels, WT:  $n = 9$ ; KO:  $n = 7$ . \*\* $P < 0.01$ . In **b** and **c**, the horizontal line represents the median, the boxes encompass the first to third quartiles, and the whiskers represent the minimum and maximum values.

and **Supplementary Fig. 7a,b**), although only connectivity with the hippocampus and nucleus accumbens remained significant ( $P < 0.05$ , corrected) after correction for multiple comparisons. These findings demonstrate that deficient synaptic multiplicity in *Cx3cr1*<sup>KO</sup> mice is associated with widespread deficits in long-range functional brain connectivity.

#### Impaired social interaction and increased repetitive behavior

Given that reduced long-range functional brain connectivity has been reported consistently in many neurodevelopmental disorders, including autism<sup>5–7,9,11,12</sup>, we investigated whether *Cx3cr1*<sup>KO</sup> mice showed alterations in social and repetitive behaviors, two phenotypes that are

observed in autism, as well as other neuropsychiatric and neurodevelopmental disorders. First we tested juvenile mice during the period when maximal deficits in synaptic pruning are observed in *Cx3cr1*<sup>KO</sup> mice<sup>19</sup>. We separated juvenile mice from their mother and placed them individually into one corner of a novel testing chamber containing clean bedding except where soiled bedding from their home cage had been placed in the opposite corner (**Supplementary Fig. 8a**). Both wild-type and *Cx3cr1*<sup>KO</sup> mice spent significantly more time in the corner with the soiled bedding than in all other corners during the 3-min initial testing period, with no significant interaction between genotype and corner preference (analysis of variance (ANOVA); corner  $\times$  genotype:  $F_{3,112} = 0.49$ ,  $P = 0.7$ ; **Fig. 4a**). These data demonstrate an intact ability to detect and respond to familiar olfactory cues in knockout mice. Next we placed wire mesh tubes into the right and

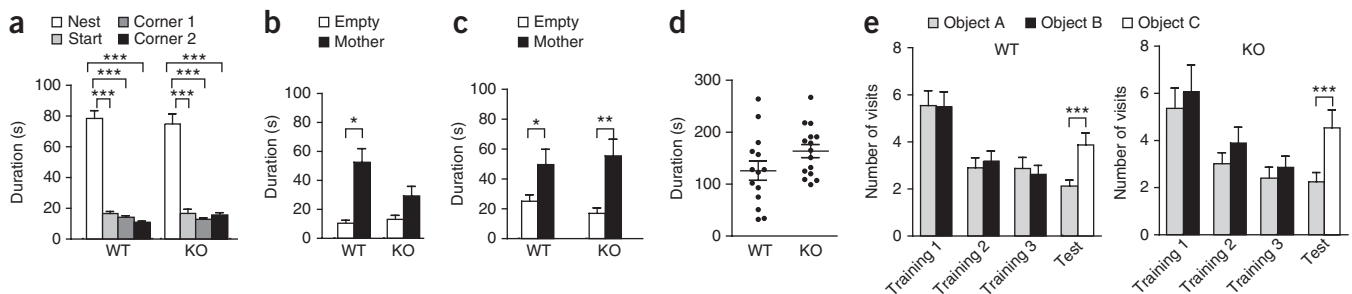


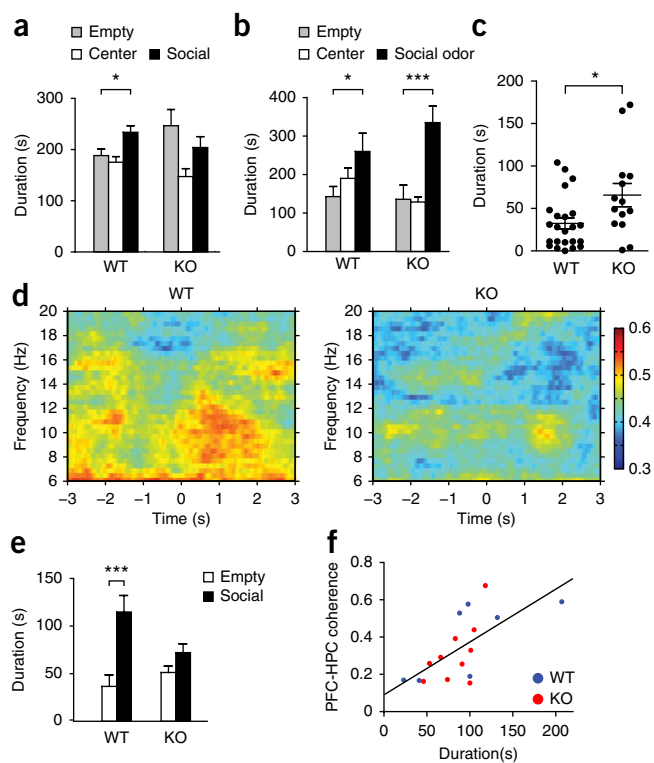
**Figure 4** Decreased social interaction in young *Cx3cr1*<sup>KO</sup> mice. **(a)** Time spent in each corner during the nest homing test by wild-type and *Cx3cr1*<sup>KO</sup> littermates (WT:  $n = 15$ ; KO:  $n = 15$ ; Bonferroni corrected). **(b)** Time the wild-type and *Cx3cr1*<sup>KO</sup> mice spent actively exploring the tube containing their mother compared to the empty tube (WT:  $n = 42$ ; KO:  $n = 30$ ; Fisher's least significant difference (LSD) test). **(c)** As in **b**, but in this case, the mother was briefly anesthetized before placement in the tube (WT:  $n = 14$ ; KO:  $n = 15$ ; Fisher's LSD test). **(d)** Self-grooming time of juvenile mice that were placed into a cage with fresh bedding scored during 10 min (*t* test; WT:  $n = 14$ ; KO:  $n = 15$ ;  $t_{27} = 1.7$ ,  $P = 0.1$ ). **(e)** Active exploration of two objects with identical shape, color and odor (objects A and B) by juvenile mice that were placed repeatedly for 3 min into a novel open area containing the two objects (training 1–3). The final trial (Test) measured active exploration after object B was replaced with an object of novel shape, color and odor (object C) (WT:  $n = 38$ ; KO:  $n = 28$ ). \* $P < 0.05$ , \*\* $P < 0.01$ , \*\*\* $P < 0.001$ , Bonferroni corrected. Error bars (**a–e**), s.e.m.

**Figure 5** Decreased social interaction and blunted functional connectivity modulation in adult *Cx3cr1*<sup>KO</sup> mice. **(a)** Exploration times of two tubes, one empty and one containing a juvenile same-sex mouse (social), by wild-type mice and *Cx3cr1*<sup>KO</sup> littermates (WT:  $n = 21$ ; KO:  $n = 15$ ; Fisher's LSD test). **(b)** Exploration times of two tubes, one empty and one containing soiled bedding from the home cage of a juvenile mouse, by wild-type mice and *Cx3cr1*<sup>KO</sup> littermates (WT:  $n = 10$ , KO:  $n = 10$ ; Fisher's LSD test). **(c)** Grooming times of *Cx3cr1*<sup>KO</sup> mice compared to wild-type littermates when placed into a novel cage with fresh bedding ( $t$  test; WT:  $n = 23$ ; KO:  $n = 14$ ;  $t_{35} = 2.5$ ,  $P = 0.02$ ). **(d)** Averaged time-dependent PFC-HPC LFP coherence during initiation of social interaction (WT:  $n = 7$ ; KO:  $n = 10$ ). Time zero corresponds to the time when the mouse touched the tube and began sniffing. Only interaction bouts longer than 3 s and preceded by no interaction for at least 3 s were included. Wild-type but not knockout mice showed a significant increase in PFC-HPC coherence in the theta band (7–12 Hz) during the first 3 s of social interaction when compared to the immediately preceding second. **(e)** Time spent investigating social and non-social stimuli in the recorded mice (WT:  $n = 7$ ; KO:  $n = 10$ ; Bonferroni corrected). **(f)** Correlation ( $r = 0.67$ ,  $P = 0.017$ ) between the duration of social interaction and PFC-HPC coherence in the theta band during the last minute of habituation. A bootstrap resampling procedure (1,000 times) gave a 95% confidence interval of 0.43–0.87, showing that the correlation was robust (**Supplementary Fig. 8d**).  $^*P < 0.05$ ,  $^{***}P < 0.001$ . Error bars (**a–c,e**), s.e.m.

left corners of the chamber, placed the animal's mother into one of the tubes and recorded exploratory activity for 5 min (**Supplementary Fig. 8a**). Wild-type mice showed a significant preference for investigating the tube containing their mother compared to the empty tube ( $P < 0.05$ ; **Fig. 4b**). In contrast, *Cx3cr1*<sup>KO</sup> littermates showed a significantly diminished preference for investigating the tube containing their mother, suggesting reduced social interest or motivation (ANOVA; corner  $\times$  genotype:  $F_{1,140} = 3.86$ ,  $P = 0.05$ ; **Fig. 4b**). Some studies have suggested that autistic individuals have difficulty understanding or inferring biological motion and intent<sup>1,32</sup>. To determine whether the reduced social interest in *Cx3cr1*<sup>KO</sup> mice was dependent on the motion of the mother, we repeated the experiment in a separate cohort of animals after brief anesthetization of the mother. In this case, both wild-type and knockout littermates showed similar, significant preferences for investigating the mother (ANOVA; corner  $\times$  genotype:  $F_{1,54} = 0.27$ ,  $P = 0.6$ ; **Fig. 4c**). These data suggest that reduced social investigation in *Cx3cr1*<sup>KO</sup> mice depends on reciprocal interaction with the mother. Repetitive and/or restricted body and hand movements are often observed in autism as well as obsessive compulsive disorder<sup>33</sup>. Thus, we assessed wild-type and *Cx3cr1*<sup>KO</sup> juvenile mice for the amount of self-grooming they performed when placed into a novel home cage for 10 min. *Cx3cr1*<sup>KO</sup> mice spent more time grooming than wild-type littermates, although the difference did not reach significance ( $P = 0.1$ ) (**Fig. 4d**).

As a further control to test the ability and motivation of knockout mice to investigate inanimate objects, we performed a novel object exploration test. We repeatedly placed juvenile wild-type and *Cx3cr1*<sup>KO</sup> littermates for 3 min into a novel open arena containing two objects of identical shape, color and odor. Exploration of both objects showed significant habituation over three trials in both wild-type and knockout mice (repeated-measures ANOVA; main effect of trial: wild type,  $F_{2,152} = 29.84$ ,  $P < 0.0001$ ; knockout,  $F_{2,108} = 18.29$ ,  $P < 0.0001$ ; **Fig. 4e**). Immediately before the final trial, we altered the shape, color and odor of one of the objects. Both wild-type and knockout mice showed a significant and similar increase in exploration of the novel object, demonstrating a similar capacity and motivation to explore inanimate objects (repeated measures ANOVA; genotype  $\times$  object:  $F_{1,65} = 0.56$ ,  $P = 0.5$ ; **Fig. 4d**).

Next we tested social interaction in adult *Cx3cr1*<sup>KO</sup> mice in a three-chambered social preference apparatus<sup>34</sup>. Mice were habituated to the



apparatus for 5 min, which was followed by a 10-min testing period in which we placed a juvenile, same-sex mouse into one of two wire mesh tubes located in the outer chambers (**Supplementary Fig. 8b**). Wild-type mice showed a significant preference for investigating the tube containing the stimulus animal compared to the empty tube (ANOVA; chamber  $\times$  genotype:  $F_{2,102} = 4.19$ ,  $P = 0.02$ ; **Fig. 5a**), whereas *Cx3cr1*<sup>KO</sup> littermates did not show a significant ( $P = 0.27$ ) preference for either tube. To control for potential deficits in olfactory discrimination and social interest, we repeated the social preference test using only soiled bedding from the juvenile mouse. Under these conditions, both genotypes showed similar social preference behavior (ANOVA; chamber  $\times$  genotype:  $F_{2,54} = 2.00$ ,  $P = 0.14$ ; **Fig. 5b**). These findings demonstrate that deficient social interaction in *Cx3cr1*<sup>KO</sup> mice persists into adulthood and, as in juvenile mice, depends on the presence of an alert, behaving social stimulus.

When placed into a novel cage, adult *Cx3cr1*<sup>KO</sup> mice spent significantly more time grooming than wild-type littermates (**Fig. 5c**), suggesting an increased propensity for spontaneous repetitive behavior under stressful conditions. We observed equivalent amounts of grooming after a brief spray of water onto the face (**Supplementary Fig. 8c**), demonstrating a similar capacity for grooming. These data show that decreased functional connectivity is associated with decreased social interaction and increased repetitive behavior, two behaviors that have been previously associated with autism and other neurodevelopmental and neuropsychiatric disorders.

### Functional connectivity predicts social interaction

The medial PFC is involved in modulating social interaction<sup>35–38</sup>, and deficits in functional connectivity between PFC and HPC have been correlated with impaired working memory in rodents<sup>25,39</sup>. To determine whether altered PFC functional connectivity in *Cx3cr1*<sup>KO</sup> mice might underlie their social interaction deficit, we measured LFP coherence between PFC and HPC during bouts of social investigation. Wild-type but not *Cx3cr1*<sup>KO</sup> mice showed a significant increase in

PFC-HPC coherence selectively in the theta band after the onset of social investigation (**Fig. 5d**; paired *t* test; wild type: percent change  $5.5 \pm 1.6\%$  (mean  $\pm$  s.e.m.),  $n = 7$ ,  $t_6 = 3.2$ ,  $P = 0.02$ ; KO: percent change  $-0.1 \pm 3.2\%$ ,  $n = 10$ ,  $t_9 = 0.25$ ,  $P = 0.8$ ). PFC and HPC theta power were not significantly altered (paired *t* test; PFC, wild type:  $n = 7$ ,  $t_6 = 1.04$ ,  $P = 0.34$ ; knockout:  $n = 10$ ,  $t_9 = 1.01$ ,  $P = 0.34$ . HPC, wild type:  $n = 7$ ,  $t_6 = 1.1$ ,  $P = 0.3$ ; knockout:  $n = 10$ ,  $t_9 = 0.52$ ,  $P = 0.61$ ) under the same conditions in either wild-type or knockout mice (**Supplementary Fig. 9a–c**), suggesting a specific correlation between behavioral state and LFP coherence.

Analysis of time spent investigating the social and non-social tube confirmed that wild-type but not knockout mice showed a significant preference for the social stimulus in the recording studies (ANOVA; chamber  $\times$  genotype:  $F_{1,30} = 6.6$ ,  $P = 0.02$ ; **Fig. 5e**). These data raise the possibility of a causal link between decreased PFC functional connectivity and deficient social interaction in the knockout mice. Such a causal link was supported by a significant correlation across both genotypes between LFP coherence in the theta band as measured during the habituation phase and time spent exploring the social stimulus during the testing phase (**Fig. 5f** and **Supplementary Fig. 9d**).

## DISCUSSION

Our findings of immature synaptic multiplicity, weak functional connectivity, impaired social interaction and increased repetitive behavior support the hypothesis that a primary deficit in microglia can impart long-term changes in gross brain wiring and behavior. Our electrophysiological data are consistent with a role for microglia in the maturation of synaptic multiplicity from an early state in which each axonal input makes few synaptic connections to a mature state in which each axonal input makes multiple connections. Although synaptic multiplicity likely contributes considerably to the reliability and experience-dependent plasticity of neuronal signaling<sup>21,40,41</sup>, its anatomical basis is not known. We speculated that MSBs targeting single neurons (MSB1s) might be a critical contributor to synaptic multiplicity in Schaffer collateral synapses and, consistent with this hypothesis, found a significant reduction in MSB1s in *Cx3cr1*<sup>KO</sup> mice (**Fig. 1j**). These data suggest a link between deficient synaptic pruning and deficient formation of MSBs and led us to propose a model in which the microglia-dependent elimination of synapses during early postnatal development is a prerequisite for the formation of strong synaptic contacts with MSB1s (**Supplementary Fig. 10**). One straightforward explanation for this phenomenon is that inactive synapses are preferentially targeted for elimination by microglia<sup>20</sup> and that MSBs preferentially emerge at active synapses. However, the failure to properly form MSB1s in *Cx3cr1*<sup>KO</sup> knockout mice in which pruning is compromised<sup>19</sup> suggests that the two phenomena are interconnected. This could occur, for example, through a homeostatic mechanism that operates to maintain optimal synapse density by promoting the addition of MSB1s to replace eliminated synapses or through the action of a secreted factor that facilitates the maturation of synapses while simultaneously licensing the elimination of neighboring synapses, as has been described at the neuromuscular junction<sup>41</sup>. Notably, the frequency of MSBs that contact different postsynaptic target neurons (MSB2s) was not different in wild-type and knockout animals (**Fig. 1k**), arguing against a general role of microglia in promoting MSBs.

Anatomical studies have reported altered microglia morphology in postmortem brain samples from individuals suffering from a variety of neurodevelopmental illnesses, including autism<sup>2</sup>, schizophrenia<sup>42</sup> and epilepsy<sup>43,44</sup>. However, it remains unclear whether these deficits are a secondary consequence of neuronal deficits or a response to environmental pathogens or whether they might represent, in at least

some cases, a primary deficit in the disorder. Our data demonstrate that a primary deficit in microglia is sufficient to induce reduced functional connectivity as assessed by electron microscopy, *in vitro* electrophysiology, *in vivo* LFP coherence and resting-state fMRI signal synchronization. These findings open the possibility that deficits in microglia-dependent synaptic pruning may be a pathological mechanism in those neurodevelopmental disorders that are characterized by weak functional connectivity, such as autism, schizophrenia and some forms of depression.

We chose to examine social investigation and novelty-induced grooming behavior in our mice because decreased functional connectivity in autism is correlated with impaired social interest and increased repetitive behavior, and these measures have been proposed as autism-related behaviors with face validity<sup>45</sup>. However, reduced functional connectivity has also been reported in other neurodevelopmental disorders, including schizophrenia<sup>7,8</sup>, epilepsy<sup>11</sup> and major depression<sup>9,10</sup>. Previous work has shown that *Cx3cr1*<sup>KO</sup> mice show deficits in maze learning<sup>23</sup>, demonstrating a role for neuron-microglia signaling in non-social cognitive functions. Further studies will be necessary to map the relationship between weak functional connectivity and behavioral deficits, but our observation of prominent deficits in long-range PFC connectivity (**Fig. 3e,g**) suggests that this region may be preferentially involved.

Our observation of a significant positive correlation between PFC-HPC functional connectivity and social investigation (**Fig. 5f**) suggests that exchange of information between PFC and other brain regions is critical for proper responding to social stimuli and is consistent with data showing that PFC is recruited by<sup>46,47</sup> and functionally required for<sup>47,48</sup> appropriate social interaction. A role for decreased long-range functional connectivity between PFC and other brain regions has been proposed in autism, schizophrenia and a variety of other disorders<sup>13</sup> on the basis of the observation that PFC functional connectivity was reduced in several studies<sup>6</sup> and correlates positively with autism clinical severity score<sup>5,49</sup>. We interpret our finding that social investigation bouts are associated with increased PFC-HPC coherence in wild-type but not knockout animals (**Fig. 5d**) to reflect an inability of knockout animals to increase information exchange between these regions, possibly as a result of their decreased baseline connectivity.

Our observation that *Cx3cr1*<sup>KO</sup> mice showed reduced exploration of alert social stimuli but no deficit in exploration driven by social olfactory cues suggests that active social interaction was a prerequisite for the behavioral phenotype (**Figs. 4b,c** and **5a,b**). Several studies have suggested that autistic subjects have difficulty in interpreting biological motion and predicting the intentions of others. For example, autistic children do not show a preference for watching correctly oriented as compared to inverted human shapes formed of moving points<sup>32</sup> and fail to elicit anticipatory throat muscle responses when reaching for food or when watching another person performing the same act<sup>50</sup>. We speculate that the reduced social interest seen in *Cx3cr1*<sup>KO</sup> mice may be the consequence of a cognitive impairment that renders social interaction with an alert partner unpredictable and/or aversive.

In summary, our findings reveal a role for microglia in promoting the maturation of circuit connectivity during development, with synapse elimination going hand in hand with enhanced synaptic multiplicity. Moreover, the association of weak synaptic multiplicity with decreased LFP coherence and BOLD synchronization in *Cx3cr1*<sup>KO</sup> mice offers a specific and testable circuit-level mechanism for the weak functional connectivity reported in autism<sup>6,13</sup> and other neurodevelopmental disorders<sup>7–12</sup>. Our data support the hypothesis that microglia-mediated synaptic pruning during development has

a critical role in sculpting neural circuit function, which may contribute to the physiological and behavioral features of a range of neurodevelopmental disorders. Our data also open the possibility that genetic and environmental risk factors for such disorders may exert their effect by modulating synapse elimination. Further studies are warranted to test the hypothesis that variation in synaptic pruning may underlie individual differences in human brain wiring and behavior.

## METHODS

Methods and any associated references are available in the [online version of the paper](#).

*Note: Any Supplementary Information and Source Data files are available in the online version of the paper.*

## AC KNOWLEDGMENTS

We thank F. Zonfrillo for expert mouse husbandry, I. Charo (University of California San Francisco) and T. Deller (University of Frankfurt) for providing mice, the EMBL Transgenic Facility for help in rederiving mouse lines, the EMBL Microscopy Facility for access to light and electron microscopes, J. Griesbach and M. Al Banchaouchi for help in videoscoring, A. Jain, J. Gordon and T. Sigurdsson for assistance in establishing *in vivo* electrophysiology, A. Galbusera for help in performing MRI acquisitions and F. D'Amato and V. Carola for advice in behavioral testing and analysis. This work was supported by funds from EMBL to C.T.G., R.C.P. and Y.Z. (Y.Z. is an EMBL Interdisciplinary Postdocs (EIPOD) fellow), the IIT to A.G., A.B. and F.S., the Italian Ministry of University and Scientific Research PRIN 2009 to D.R. and a Forschungskredit of the University of Zurich to A.L.V.

## AUTHOR CONTRIBUTIONS

Y.Z. designed, carried out and analyzed the *in vivo* electrophysiology experiments. R.C.P. designed, carried out and analyzed all non-electrophysiological behavioral experiments. A.B., F.S. and A.G. designed, carried out and analyzed the fMRI experiments. L.W. designed, carried out and analyzed the light microscopy experiment. G.B. designed and carried out the electron microscopy experiments that were analyzed together with L.W. *In vitro* electrophysiological experiments were designed, carried out and analyzed by F.P. and D.R. A.L.V. contributed the custom *in vivo* electrophysiology recording hardware and expertise. C.T.G. conceived the project and wrote the manuscript with input from Y.Z., R.C.P. and D.R.

## COMPETING FINANCIAL INTERESTS

The authors declare no competing financial interests.

Reprints and permissions information is available online at <http://www.nature.com/reprints/index.html>.

- Bourgeron, T. A synaptic trek to autism. *Curr. Opin. Neurobiol.* **19**, 231–234 (2009).
- Voineagu, I. *et al.* Transcriptomic analysis of autistic brain reveals convergent molecular pathology. *Nature* **474**, 380–384 (2011).
- Kumar, A. *et al.* A brain region-specific predictive gene map for autism derived by profiling a reference gene set. *PLoS ONE* **6**, e28431 (2011).
- Dichter, G.S. Functional magnetic resonance imaging of autism spectrum disorders. *Dialogues Clin. Neurosci.* **14**, 319–351 (2012).
- Dinstein, I. *et al.* Disrupted neural synchronization in toddlers with autism. *Neuron* **70**, 1218–1225 (2011).
- Schipul, S.E., Keller, T.A. & Just, M.A. Inter-regional brain communication and its disturbance in autism. *Front. Syst. Neurosci.* **5**, 10 (2011).
- Meyer-Lindenberg, A.S. *et al.* Regionally specific disturbance of dorsolateral prefrontal-hippocampal functional connectivity in schizophrenia. *Arch. Gen. Psychiatry* **62**, 379–386 (2005).
- Karbasforoushan, H. & Woodward, N.D. Resting-state networks in schizophrenia. *Curr. Top. Med. Chem.* **12**, 2404–2414 (2012).
- Veer, I.M. *et al.* Whole brain resting-state analysis reveals decreased functional connectivity in major depression. *Front. Syst. Neurosci.* **4** (2010).
- Marchand, W.R. *et al.* Aberrant functional connectivity of cortico-basal ganglia circuits in major depression. *Neurosci. Lett.* **514**, 86–90 (2012).
- Waites, A.B., Briellmann, R.S., Saling, M.M., Abbott, D.F. & Jackson, G.D. Functional connectivity networks are disrupted in left temporal lobe epilepsy. *Ann. Neurol.* **59**, 335–343 (2006).
- Harrison, B.J. *et al.* Altered corticostriatal functional connectivity in obsessive-compulsive disorder. *Arch. Gen. Psychiatry* **66**, 1189–1200 (2009).
- Courchesne, E. & Pierce, K. Why the frontal cortex in autism might be talking only to itself: local over-connectivity but long-distance disconnection. *Curr. Opin. Neurobiol.* **15**, 225–230 (2005).
- Frith, U. *Autism: Explaining the Enigma* (Blackwell Publishing, 2003).
- Courchesne, E., Redcay, E., Morgan, J.T. & Kennedy, D.P. Autism at the beginning: microstructural and growth abnormalities underlying the cognitive and behavioral phenotype of autism. *Dev. Psychopathol.* **17**, 577–597 (2005).
- Rubenstein, J.L.R. & Merzenich, M.M. Model of autism: increased ratio of excitation/inhibition in key neural systems. *Genes Brain Behav.* **2**, 255–267 (2003).
- Paolicelli, R.C. & Gross, C.T. Microglia in development: linking brain wiring to brain environment. *Neuron Glia Biol.* **7**, 77–83 (2011).
- Kierdorf, K. *et al.* Microglia emerge from erythromyeloid precursors via Pu.1- and Irf8-dependent pathways. *Nat. Neurosci.* **16**, 273–280 (2013).
- Paolicelli, R.C. *et al.* Synaptic pruning by microglia is necessary for normal brain development. *Science* **333**, 1456–1458 (2011).
- Schafer, D.P. *et al.* Microglia sculpt postnatal neural circuits in an activity and complement-dependent manner. *Neuron* **74**, 691–705 (2012).
- Hsia, A.Y., Malenka, R.C. & Nicoll, R.A. Development of excitatory circuitry in the hippocampus. *J. Neurophysiol.* **79**, 2013–2024 (1998).
- He, L. *et al.* Compound vesicle fusion increases quantal size and potentiates synaptic transmission. *Nature* **459**, 93–97 (2009).
- Rogers, J.T. *et al.* CX3CR1 deficiency leads to impairment of hippocampal cognitive function and synaptic plasticity. *J. Neurosci.* **31**, 16241–16250 (2011).
- Sorra, K.E. & Harris, K.M. Occurrence and three-dimensional structure of multiple synapses between individual radiatum axons and their target pyramidal cells in hippocampal area CA1. *J. Neurosci.* **13**, 3736–3748 (1993).
- Sigurdsson, T., Stark, K.L., Karayiorgou, M., Gogos, J.A. & Gordon, J.A. Impaired hippocampal-prefrontal synchrony in a genetic mouse model of schizophrenia. *Nature* **464**, 763–767 (2010).
- Schwarz, A.J. *et al.* The low-frequency blood oxygenation level-dependent functional connectivity signature of the hippocampal-prefrontal network in the rat brain. *Neuroscience* **228**, 243–258 (2013).
- Sforzini, F., Schwarz, A.J., Galbusera, A., Bifone, A. & Gozzi, A. Distributed BOLD and CBV-weighted resting-state networks in the mouse brain. *Neuroimage* doi:10.1016/j.neuroimage.2013.09.050 (29 September 2013).
- Gozzi, A. *et al.* A neural switch for active and passive fear. *Neuron* **67**, 656–666 (2010); erratum **73**, 854 (2012).
- Liu, X., Zhu, X.-H., Zhang, Y. & Chen, W. Neural origin of spontaneous hemodynamic fluctuations in rats under burst-suppression anesthesia condition. *Cereb. Cortex* **21**, 374–384 (2011).
- Steffey, M.A., Brosnan, R.J. & Steffey, E.P. Assessment of halothane and sevoflurane anesthesia in spontaneously breathing rats. *Am. J. Vet. Res.* **64**, 470–474 (2003).
- Hoover, W.B. & Vertes, R.P. Anatomical analysis of afferent projections to the medial prefrontal cortex in the rat. *Brain Struct. Funct.* **212**, 149–179 (2007).
- Klin, A., Lin, D.J., Gorrindo, P., Ramsay, G. & Jones, W. Two-year-olds with autism orient to non-social contingencies rather than biological motion. *Nature* **459**, 257–261 (2009).
- American Psychiatric Association. *Diagnostic and Statistical Manual of Mental Disorders, 4th Edn., Text Revision (DSM-IV-TR)* (American Psychiatric Association, 2000).
- Nadler, J.J. *et al.* Automated apparatus for quantitation of social approach behaviors in mice. *Genes Brain Behav.* **3**, 303–314 (2004).
- Adolphs, R. Conceptual challenges and directions for social neuroscience. *Neuron* **65**, 752–767 (2010).
- Courchesne, E. *et al.* Mapping early brain development in autism. *Neuron* **56**, 399–413 (2007).
- Gläscher, J. *et al.* Lesion mapping of cognitive control and value-based decision making in the prefrontal cortex. *Proc. Natl. Acad. Sci. USA* **109**, 14681–14686 (2012).
- Uylings, H.B.M., Groenewegen, H.J. & Kolb, B. Do rats have a prefrontal cortex? *Behav. Brain Res.* **146**, 3–17 (2003).
- Barker, G.R.I. & Warburton, E.C. When is the hippocampus involved in recognition memory? *J. Neurosci.* **31**, 10721–10731 (2011).
- LaMantia, A.S. & Rakic, P. Axon overproduction and elimination in the corpus callosum of the developing rhesus monkey. *J. Neurosci.* **10**, 2156–2175 (1990).
- Barber, M.J. & Lichtman, J.W. Activity-driven synapse elimination leads paradoxically to domination by inactive neurons. *J. Neurosci.* **19**, 9975–9985 (1999).
- Fillman, S.G. *et al.* Increased inflammatory markers identified in the dorsolateral prefrontal cortex of individuals with schizophrenia. *Mol. Psychiatry* **18**, 206–214 (2013).
- Crespel, A. *et al.* Inflammatory reactions in human medial temporal lobe epilepsy with hippocampal sclerosis. *Brain Res.* **952**, 159–169 (2002).
- Pernot, F. *et al.* Inflammatory changes during epileptogenesis and spontaneous seizures in a mouse model of mesiotemporal lobe epilepsy. *Epilepsia* **52**, 2315–2325 (2011).
- Crawley, J.N. Mouse behavioral assays relevant to the symptoms of autism. *Brain Pathol.* **17**, 448–459 (2007).
- Amodio, D.M. & Frith, C.D. Meeting of minds: the medial frontal cortex and social cognition. *Nat. Rev. Neurosci.* **7**, 268–277 (2006).
- Avale, M.E. *et al.* Prefrontal nicotinic receptors control novel social interaction between mice. *FASEB J.* **25**, 2145–2155 (2011).
- Yizhar, O. *et al.* Neocortical excitation/inhibition balance in information processing and social dysfunction. *Nature* **477**, 171–178 (2011).
- Bartfeld, P. *et al.* A big-world network in ASD: dynamical connectivity analysis reflects a deficit in long-range connections and an excess of short-range connections. *Neuropsychologia* **49**, 254–263 (2011).
- Cattaneo, L. *et al.* Impairment of actions chains in autism and its possible role in intention understanding. *Proc. Natl. Acad. Sci. USA* **104**, 17825–17830 (2007).

## ONLINE METHODS

**Animals.** Animals were group housed and kept on a 12 h light, 12 h dark cycle (lights on at 7 a.m.) with constant ambient temperature ( $21.5 \pm 1$  (range) °C) and humidity ( $55 \pm 8\%$ ) and food and water available *ad libitum*. Mice were produced by intercrossing *Thy1::GFP Thy1::GFP; Cx3cr1<sup>KO/+</sup>* mice<sup>51</sup>. *Cx3cr1<sup>KO</sup>* and *Thy1::GFP-M* mice were kindly provided by I. Charo<sup>52</sup> and T. Deller<sup>51</sup>, respectively. All juvenile behavioral tests were performed while mice were housed with dam and littermates. Both male and female mice were used in all juvenile behavioral tests. Only male mice were used for the LFP recordings and adult behavior tests. All mice were on a C57BL/6J congenic background. Mice were bred, genotyped and tested at EMBL following protocols approved by the Italian Ministry of Health. Fluorescent flow cytometry of peripheral blood was used to distinguish homozygous from heterozygous *Thy1::GFP* mice.

**Maternal homing test.** Two independent cohorts (P15–P18 and P21–P24) of *Cx3cr1<sup>KO</sup>* and control littermates were subjected to a maternal homing test<sup>53</sup> that exploits the tendency of juvenile mice to maintain body contact with the mother and their siblings and tests olfactory, visual and motor capacities. Mice were separated from the mother for at least 30 min before testing. During habituation, individual pups were transferred to a Plexiglas arena (50 × 50 cm, walls 30 cm high) containing fresh bedding with a small amount of soiled bedding (not including fecal boli) sprinkled into the opposite corner and allowed to explore for 3 min. Total time spent in the starting, nest and neutral corners was measured using a videotracking system (Videomot, TSE Systems, Bad Homburg, Germany). Subsequently, the mice were briefly removed to a holding cage while two wire-mesh tubes were placed into the neutral corners, one containing the animal's mother. Time spent sniffing the tubes (empty and mother) was scored from videotape for 5 min after placement of the mouse back into the chamber (Observer XT, Noldus Information Technology, Wageningen, Netherlands).

**Novel object recognition test.** Juvenile (P18–P22, after the maternal homing testing) mice were individually placed in a Plexiglas arena (50 × 50 cm, walls 30 cm high) for 5 min, and exploration was quantified by videotracking (Videomot). Subsequently, mice were subjected to three habituation sessions in which two objects identical in shape, color and odor were introduced into the arena (3 min, with a 2 min intertrial interval). The mouse was placed in a holding cage between sessions. Before the last session, one of the objects was replaced with a novel object. Time spent in active exploration of each object was scored during each session from the videotape (Observer XT). The arena and objects were cleaned with H<sub>2</sub>O and 70% EtOH after each session.

**Grooming test.** Juvenile (P25–P28) or adult mice were individually placed in a standard cage containing a thin layer of fresh bedding, and the total time spent performing face, body and/or tail grooming was scored during minutes 5–15 as described in ref. 54. At the end of the test, a small quantity of water was sprayed onto the face of the mouse, and the total time spent grooming was recorded during 1 min. The experimenter was blind to the animal genotype when assessing grooming behavior.

**Social preference test.** After habituation to the room for at least 30 min, mice (2–4 months old) were placed into a three-compartment social approach apparatus<sup>34</sup> and allowed to explore for 5 min. Mice were briefly constrained under an opaque Plexiglas tube in the center compartment while wire-mesh tubes were placed into the outside compartments away from the door, and a same-sex juvenile (P21–P24) mouse was placed into one of the two tubes. After removal of the opaque tube, the total time spent in the social and non-social compartments was determined using videotracking (Videomot).

**In vivo electrophysiology.** Wild-type and *Cx3cr1<sup>KO</sup>* littermates (3–5 months old) were implanted with depth electrodes, and LFPs were recorded with a wireless Neurologger 2A device<sup>55,56</sup> mounted on the head of the animal. Electrode implantation was carried out in anesthetized mice (100 mg per kg body weight ketamine and 10 mg per kg body weight xylazine supplemented with halothane as needed) using a stereotaxic frame (Kopf Instruments, Tujunga, CA) following previously published protocols<sup>57</sup>. Briefly, an incision was cut above the mouse skull, and burr holes were drilled (dorsal HPC: 1.9 mm posterior and 1.4 mm lateral from bregma, 1.35 mm depth from brain surface; ventral HPC: 3.2 mm

posterior and 3.1 mm lateral from bregma, 3.85 mm depth; PFC: 1.8 mm anterior and 0.5 mm lateral to the right from bregma, 1.5 mm depth) to facilitate implantation of tungsten wire electrodes (Teflon coated, 0.075 mm diameter, Advent Research Materials, Oxford, UK). Screws anchored at the posterior and anterior region of the skull served as the ground and reference, respectively. Electrode wires were inserted into a seven-pin connector that served as an interface for the Neurologger 2A recording device, and dental cement was carefully applied over the skull to form a protective head stage. After surgery, animals were housed individually and allowed to recover for at least 1 week before testing. The behavior of the mice was recorded and tracked using Viewer2 software (Bioobserve, St. Augustin, Germany). The speed of the animal was calculated from the tracking files and smoothed using a LOWESS method<sup>58</sup>. Power and coherence spectra at a speed of 0–5 cm s<sup>-1</sup> were extracted from the LFP data collected during the habituation phase of the three-compartment social approach test. Data were acquired at 1,600 Hz and analyzed offline using multi-taper spectral analysis (time-frequency bandwidth;  $TW = 3$ ,  $K = 5$  tapers; Chronux toolbox<sup>59</sup>) with custom Matlab scripts after segmentation into 1-s trials. The analysis of time-dependent coherence during social interaction used the 3 s before the interaction start and the 3 s after it with  $TW = 4$  and  $K = 6$ . The moving window length was 2 s with 50-ms steps. Power was calculated as the sum of the power within each frequency band, and coherence was calculated as the mean within each frequency band. At the end of the experiments, electrolytic lesions were made around the electrode tip to verify the position of implantation in the brain.

**In vitro electrophysiology.** Hippocampal slices were prepared from wild-type and *Cx3cr1<sup>KO</sup>* littermates at P38–P40. Animals were decapitated after being anesthetized with halothane, and whole brains were rapidly immersed for 10 min in ice-cold continuously oxygenated (95% O<sub>2</sub>, 5% CO<sub>2</sub>; pH 7.4) glycerol solution containing 2.5 mM KCl, 2.4 mM CaCl<sub>2</sub>, 1.2 mM MgCl<sub>2</sub>, 1.2 mM NaHPO<sub>4</sub>, 26 mM NaHCO<sub>3</sub>, 11 mM glucose and 250 mM glycerol. Transverse 250- $\mu$ m slices were cut at 4 °C with a vibratome (DSK, Kyoto, Japan) in oxygenated glycerol solution and allowed to recover for 1 h in oxygenated artificial cerebrospinal fluid (ACSF) containing 125 mM NaCl, 2.5 mM KCl, 2.0 mM CaCl<sub>2</sub>, 1.0 mM MgCl<sub>2</sub>, 1.25 mM NaH<sub>2</sub>PO<sub>4</sub>, 26 mM NaHCO<sub>3</sub> and 10 mM glucose. Individual slices were transferred to the recording chamber and superfused with oxygenated ACSF at 1.5 ml per min at room temperature (23–25 °C). Neurons were visualized with an upright Axioscope microscope (Zeiss, Jena, Germany). Patch-clamp recordings were obtained using borosilicate glass electrodes (4–5 M) filled with an intracellular solution containing 135 mM Cs-methanesulphonate, 7 mM CsCl, 2 mM MgCl<sub>2</sub>, 10 mM 4-(2-hydroxyethyl)-1-piperazineethanesulfonic acid, 2 mM MgATP, 0.3 mM NaGTP and 5 mM 1,2-bis-(*o*-aminophenoxy)-ethane-*N,N,N,N*-tetraacetic acid equilibrated to pH 7.3 with CsOH. Neurons were clamped at –70 mV for sEPSC and mEPSC recordings and at 0 mV for mIPSC recordings. For experiments comparing sEPSCs and mEPSCs, each cell was derived from a different slice. We applied TTX (0.5–1 mM) for at least 8 min before recording mEPSCs and mIPSCs. Membrane currents, recorded with a patch-clamp amplifier (Axopatch 200A, Molecular Devices, Foster City, CA), were filtered at 2 kHz, digitized (10 kHz) and acquired with Clampex 10 software (Molecular Devices). Neuron passive properties and noise amplitude were assessed in all recordings (**Supplementary Fig. 1a–g**). Recorded signals were low-pass filtered at 1 kHz and analyzed using Clampfit 10 software (Molecular Devices). Excitatory synaptic currents were identified on the basis of a template created for each neuron using 30–50 single events for each trace. All events recognized through the template search function were visualized, identified and accepted by manual analysis. Cumulative distributions for single neurons and recording conditions were obtained by pooling together 150–400 single synaptic currents. The recording was not performed blind to the animal genotype. Data were derived from the following cells/slices/mice: EPSC amplitude, WT:  $n = 14/14/5$ ; KO:  $n = 9/9/5$ ; EPSC frequency, WT, P15:  $n = 20/17/4$ , P40:  $n = 16/16/5$ ; KO, P15:  $n = 26/16/5$ , P40:  $n = 12/12/5$ .

**Immunohistochemistry.** Mice were anesthetized intraperitoneally with Avertin (Sigma-Aldrich, St. Louis, MO) and perfused transcardially with 4% formaldehyde. Transverse 40- $\mu$ m sections were cut on a vibratome (Leica Microsystems, Wetzlar, Germany), permeabilized in PBS with 1% Triton (1 h at 37 °C) and blocked with PBS with 0.5% Triton, 1% bovine serum albumin and 5% normal goat serum (1 h at 37 °C). Axonal neurofilaments were immunodetected by

incubation with primary mouse anti-NF200 (MAB5262, Millipore, Temecula, CA; 1:400, overnight at 37 °C) followed by incubation with secondary antibody (goat, Alexa Fluor 568, A11004, Life Technologies, Carlsbad, CA; 1:800, 2 h at room temperature). Images were acquired on an SP5 confocal microscope (Leica Microsystems). Axonal density was assessed in the CA1 stratum radiatum of the hippocampus by manually counting the number of axons passing through a volume of  $31 \times 31 \times 7.8 \mu\text{m}$ ,  $100 \mu\text{m}$  distant from the stratum pyramidale and  $100 \mu\text{m}$  from the CA1 boundary defined by dense *Thy1::GFP* expression. Images were processed using NIH ImageJ software. Quantifications were manually performed by an experimenter who was blind to genotype.

**Electron microscopy.** Three brains of each genotype were perfused and fixed with 2% (wt/vol) paraformaldehyde and 2.5% (wt/vol) glutaraldehyde (TAAB) in 0.1 M Na-cacodylate buffer, pH 7.1. Hippocampal stratum radiatum areas were dissected from 500- $\mu\text{m}$ -thick vibratome sections and post-fixed in 1% (wt/vol)  $\text{OsO}_4$  supplemented with 1.5% (wt/vol) potassium ferrocyanide for 2 h. Samples were subsequently dehydrated in ethanol and infiltrated with propylene oxide and Epon (1:1) followed by resin embedding. Ultrathin (50 nm) sections were cut (Ultracut S, Leica Microsystems)  $100 \mu\text{m}$  away from the CA1 pyramidal cell body layer, counterstained with uranyl acetate and lead citrate and observed with a Jeol 1010 transmission electron microscope (Jeol, Tokyo, Japan) equipped with a MSC 791 charge-coupled device camera (Gatan, Pleasanton, CA). Synaptic vesicles were quantified from single electron micrographs. Docked vesicles were counted as those vesicles directly adjacent to the synaptic membrane, whereas reserve vesicles were counted as those within 50 nm of the membrane. The proportion of single-synapse boutons as compared to MSBs was first assessed from single micrographs regardless of the origin of the contacted spines. A single synapse bouton was defined as a presynaptic element synapsing onto a single spine, whereas an MSB was identified as a presynaptic element synapsing onto at least two spines. The proportion of single-synapse boutons as compared to MSB1s or MSB2s was subsequently assessed by following contacted spines through an independent set of reconstructed serial sections containing eight consecutive micrographs. Synapses that appeared perforated were found in equal frequency in wild-type and knockout mice (data not shown) but were excluded from the analysis, as they could not be unambiguously categorized. Quantifications were manually performed by an experimenter who was blind to genotype.

**fMRI acquisition and data analyses.** MRI experiments were performed on *Cx3cr1<sup>KO</sup>* mice (26–38 g, 19–24 weeks of age) and wild-type littermates (25–37 g, 19–23 weeks of age) bred at EMBL. The animal preparation protocol was adapted from previous studies<sup>27,28,60</sup> and optimized for physiological stability. Mice were anesthetized with isoflurane (5%), intubated and artificially ventilated. The left femoral artery was cannulated for contrast agent administration, continuous blood pressure monitoring, infusion of paralyzing agent (gallamine triethiodide, 20 mg per kg body weight per h; Sigma-Aldrich, Milano, Italy) and blood sampling. Because deep isoflurane anesthesia (>1.8%) could produce bursts of high-voltage slow waves separated by suppression periods that appeared to be correlated with resting hemodynamic activity<sup>29</sup>, isoflurane was used for the surgical procedures only. fMRI experiments were done under shallow, accurately controlled halothane anesthesia (0.7%)<sup>27</sup>. To minimize any carryover effects, the anesthetic switch took place 90 min before the beginning of resting-state fMRI (rsfMRI) image acquisition. Arterial blood gases ( $p_a\text{CO}_2$  and  $p_a\text{O}_2$ ) were measured as  $20.0 \pm 3.0$  mm (mean  $\pm$  s.e.m.) Hg ( $p_a\text{CO}_2$ ) and  $280 \pm 12$  mm Hg ( $p_a\text{O}_2$ ), and  $24.2 \pm 5.2$  mm Hg ( $p_a\text{CO}_2$ ) and  $281 \pm 25$  mm Hg ( $p_a\text{O}_2$ ) for *Cx3cr1<sup>KO</sup>* mice and wild-type littermates, respectively. All experiments were performed using a 7.0 Tesla MRI scanner (Bruker Biospin, Milan, Italy). Transmission and reception were achieved using a 72-mm birdcage transmit coil and a custom-built saddle-shaped solenoid coil for signal reception. Shimming was performed on a  $6 \times 6 \times 6$  mm region using a FASTMAP protocol. For each session, high-resolution anatomical images were acquired with a fast-spin echo sequence (RARE) with the following parameters: repetition time (TR)/echo time (TE) 5,500/60 ms, matrix  $192 \times 192$ , field of view  $2 \times 2 \text{ cm}^2$ , 24 coronal slices, slice thickness 0.50 mm. Co-centered single-shot BOLD rsfMRI time series were acquired using an echo planar imaging (EPI) sequence with the following parameters: TR/TE 1,000/15 ms, flip angle 60°, matrix  $100 \times 87$ , field of view  $2.3 \times 2 \text{ cm}^2$ , 16 coronal slices, slice thickness 0.75 mm, 360 volumes, and a total rsfMRI acquisition time of

6 min. Image time series data were preprocessed with tools from fMRI of the brain (Oxford FMRIB Software Library, FSL, <http://www.fmrib.ox.ac.uk/fsl>)<sup>61</sup>, analysis of functional neuroimages (AFNI, <http://afni.nimh.nih.gov/>) software<sup>62</sup> and MATLAB using the following processing pipeline. First, the anatomical images were linearly (12 degrees of freedom) normalized to an MRI anatomical template of the mouse brain using FSL's FLIRT, and the generated transformation matrices were applied to the co-centered rsfMRI time series. The normalized data had a spatial resolution of  $0.1 \times 0.1 \times 0.5 \text{ mm}^3$  ( $192 \times 192 \times 24$  matrix). After co-registration, all the functional images were realigned (correction for motion), and the six head-motion traces were regressed from the time series data (AFNI). To minimize non-neural signal contributions, the mean ventricular signal (averaged fMRI time course within a manually drawn ventricle mask) was considered as nuisance signal and regressed out of each of the time series for each subject. Finally, the image time series were bandpass filtered to a frequency window of 0.01–0.08 Hz (AFNI) and spatially smoothed using a Gaussian kernel of full width at half maximum of 0.6 mm. Small a priori seed regions of  $3 \times 3 \times 1$  voxels were chosen on the basis of anatomical structures belonging to networks of interest. To map the connectivity relationships with the prelimbic cortex at a high spatial resolution, a reference seed (distance to bregma  $\approx 1.94$  mm) was used to generate a whole-brain correlation map using the mean time course from the seed as a regressor for each voxel using AFNI. Individual subject correlation maps were transformed to normally distributed  $z$  scores using Fisher's  $r$ -to- $z$  transformation before assessing consistent group level connectivity distributions using one-sample  $t$  tests. Resulting group maps were thresholded at  $|Z| > 1.7$ , followed by a cluster-level multiple comparison correction at a significance level of  $P < 0.01$  (FSL). For each rsfMRI time series, the mean time course from each seed was calculated and variance normalized (AFNI). All-pairs correlation coefficients (the zeroth lag of the normalized covariance function) were then calculated to generate seed-seed correlation matrices for each subject. Mean correlation matrices for the full cohort were calculated, as well as one-sample  $T$ -statistic matrices indicating the strength of the correlation relative to zero. The latter were thresholded at  $P = 0.05$  and corrected for multiple comparisons with a false discovery rate of  $q = 0.05$  using Benjamini-Hochberg's procedure. To illustrate the different connective architecture of the two cohorts of mice, a graph representation of the connectivity matrices was generated using the software Pajek (version 3.2, <http://pajek.imfm.si/doku.php>) by thresholding correlation coefficients at  $|r| > 0.1$ .

**Statistical analyses.** All data are represented as the mean  $\pm$  s.e.m. For statistical analyses of vesicles and axons, unpaired  $t$  test was performed. Synaptic multiplicity (sEPSC/mEPSC) was evaluated using paired  $t$  test. The proportions of single synapse boutons as compared to MSBs, MSB1s or MSB2s were statistically analyzed using  $\chi^2$  test. Cumulative probability plots of the amplitude and interevent interval of synaptic currents were compared with the Kolmogorov-Smirnov two-sample test based on distributions obtained using 100 events from each cell, and for comparison of means,  $t$  test was used.  $t$  test, ANOVA and repeated-measure ANOVA were used for statistical analyses of behavioral data. For ANOVA, *post-hoc* tests were done using either Bonferroni correction or Fisher's LSD test. For comparison of LFP data between genotypes at different frequency bands,  $t$  test was used. Paired  $t$  test was used for theta coherence before and after the start of social interaction. No statistical methods were used to predetermine sample sizes, but our sample sizes are similar to those reported in previous publications<sup>19,25,27,54</sup>. Data collection and processing were randomized or performed in a counter-balanced manner.

- Feng, G. *et al.* Imaging neuronal subsets in transgenic mice expressing multiple spectral variants of GFP. *Neuron* **28**, 41–51 (2000).
- Haskell, C.A. *et al.* Targeted deletion of CX3CR1 reveals a role for fractalkine in cardiac allograft rejection. *J. Clin. Invest.* **108**, 679–688 (2001).
- Scattoni, M.L., Puopolo, M., Calamandrei, G. & Ricceri, L. Basal forebrain cholinergic lesions in 7-day-old rats alter ultrasound vocalisations and homing behaviour. *Behav. Brain Res.* **161**, 169–172 (2005).
- Silverman, J.L., Tolu, S.S., Barkan, C.L. & Crawley, J.N. Repetitive self-grooming behavior in the BTBR mouse model of autism is blocked by the mGluR5 antagonist MPEP. *Neuropsychopharmacology* **35**, 976–989 (2010).
- Brankač, J., Kukushka, V.I., Vyssotski, A.L. & Draguhn, A. EEG gamma frequency and sleep-wake scoring in mice: comparing two types of supervised classifiers. *Brain Res.* **1322**, 59–71 (2010).

56. Vyssotski, A.L. *et al.* EEG responses to visual landmarks in flying pigeons. *Curr. Biol.* **19**, 1159–1166 (2009).
57. Adhikari, A., Topiwala, M.A. & Gordon, J.A. Synchronized activity between the ventral hippocampus and the medial prefrontal cortex during anxiety. *Neuron* **65**, 257–269 (2010).
58. Drai, D. & Golani, I. SEE: a tool for the visualization and analysis of rodent exploratory behavior. *Neurosci. Biobehav. Rev.* **25**, 409–426 (2001).
59. Mitra, P. & Bokil, H. *Observed Brain Dynamics* (Oxford University Press, New York, 2008).
60. Ferrari, L. *et al.* A robust experimental protocol for pharmacological fMRI in rats and mice. *J. Neurosci. Methods* **204**, 9–18 (2012).
61. Smith, S.M. *et al.* Advances in functional and structural MR image analysis and implementation as FSL. *Neuroimage* **23** (suppl. 1), S208–S219 (2004).
62. Cox, R.W. AFNI: software for analysis and visualization of functional magnetic resonance neuroimages. *Comput. Biomed. Res.* **29**, 162–173 (1996).

